CrossMark

ORIGINAL ARTICLE

Stability evaluation method for hyperbolic coal pillars under the coupling effects of high temperature and ground stress

Huaizhan Li[1,2] · Guangli Guo[1,2] · Jianfeng Zha[1,2] · Yan He[3] · Zhiyong Wang[1,2] · Shuangyu Qin[1,2]

Abstract We studied an underground coal gasification technique using strip mining-face mining gasifier controlled retraction injection technology (SMFM). This green mining approach offers several advantages over conventional strip mining but the stress distribution and stability of SMFM operations remain largely untested. In particular, hyperbolic coking pillars are used in SMFM compared with rectangular pillars used in traditional strip mining, which can influence the ultimate bearing capacity and stability. We use numerical simulations to investigate the influence of different factors (arch height, pillar height and width, mechanical characteristics), under the coupling effect of high temperature, on the ultimate bearing capacity of hyperbolic pillars. Our results indicate that arch height has a strong influence on pillar stress, while changes in pillar width and height are less significant. A stability evaluation method is proposed and tested on a case study in Inner Mongolia. Our theoretical results have practical significance for the promotion and application of SMFM.

Introduction

Underground coal gasification (UCG) technology controls underground coal combustion processes and produces combustible gas using thermal and chemical reactions. As a green mining method, UCG extracts energy from coal resources using a gasification process and leaves tailings (e.g., ash and gangue) in a combustion area. This new technology, which integrates shaft building, coal mining, and gasification configurations, is considered a second generation mining method of developing clean energy and chemical materials, and can be applied to different disciplines (Zamzow 2010; Khadse et al. 2007; Shafirovich and Varma 2009; Bhutto et al. 2013; Yang et al. 2008; Prabu and Jayanti 2011, 2012; Stanczyk et al. 2011; Mcinnis et al. 2016).

UCG technology has the capacity to exploit coal resources left over by conventional mining with the benefits of higher safety, fewer contaminants, and low required investment. Compared with conventional mining, UCG offers valuable advantages in controlling the gasification working face, minimizing mining-induced environmental problems, and producing valuable clean energy and chemical materials required for economic development. Moreover, by combining strata movement theory and control technology, UCG provides access to coal resources with high recovery difficulty or low economic value, including those buried under buildings, railways and water bodies, as well as thin and deep coal seams. The development of UCG technology is therefore not only important

✉ Guangli Guo
  guo_gl123@163.com

  Huaizhan Li
  lh_zhan@163.com

1 School of Environment Science and Spatial Informatics, China University of Mining and Technology, Xuzhou 221116, Jiangsu, China

2 Key Laboratory for Land Environment and Disaster Monitoring of SBSM, China University of Mining and Technology, Xuzhou 221116, Jiangsu, China

3 ENN Group, Langfang 065000, Hebei, China

for protecting the environment, but also of great practical and long-term significance for the international coal industry to manage market demand and carbon supply.

The concept of UCG was first put forward by the German scientist, Sir William, in 1868 (Siemens 1868). After more than a century of effort by scholars worldwide, the first experimental UCG workstation was established in Uzbekistan in 1961 (Klimenko 2009). Studies were conducted during that time by the former USSR, USA, and others (Derbin et al. 2015; Stuermer et al. 1982; Shafirovich and Varma 2009). However, many disadvantages remained including an excessive number of gasification boreholes, high gasifier costs, and higher requirements from the surrounding geological and hydrological conditions. By 1976, a controlled retraction injection (CRI) point gasification technique was proposed by Lawrence Livermore National Laboratory, which greatly promoted the development of UCG technology (Couch 2009). At present, the world's primary UCG operations include the Chinchilla in Australia (Walker et al. 2001), Angren in Uzbekistan, and Majuba in South Africa (Shafirovich and Varma 2009). Industrial UCG experiments are also actively carried out in several Chinese coal mines including the Xuzhou Mazhuang, Tangshan Liuzhuang, Chongqing Zhongliangshan Northern, Huating, and Matigou (Yang et al. 1998, 2000; Wang et al. 2008; Xin et al. 2013; Xin 2014).

Strip mining involves the division of a mining area into formal strips, some of which are actively mined. The core issue of strip mining design is the stability of coal pillars. Strip coal pillars can usually support the load of overlying strata, which may move and deform during operation, and control surface subsidence (Guo et al. 2016; Gao 2014; Li et al. 2016). Wilson established the well-known strip coal pillar design formula based on pillar yielding capacity using a mechanical model (two zone constraint theory), which has become a classic method of strip coal pillar design. At present, the most widely used evaluation method of coal pillar stability is the safety factor method.

Conventional mining employs rectangular and primary coal pillars, while the UCG arrangement of strip mining-face mining gasifier CRI underground gasification technology, hereafter referred to as SMFM, uses hyperbolic coking (i.e., semi-coking) pillars. Differences in the mechanical properties of pillar structures lead to different bearing mechanisms, deformation characteristics, and influence the pillar stress distribution, safety, stability, and capacity. Temperatures in the gasifier can reach up to 1400 °C (Tang 2013), which can also influence the bearing capacity. As a consequence, problems with the large-scale popularization and application of UCG technology are likely to occur. For example, the separated coal pillars should be reduced to improve resource utilization, and the geometric parameters of the gasifier should be optimized to control the destruction of overlying strata in the combustion cavity and surface subsidence, as well as to protect the ground environment.

The development of modern directional borehole and UCG technologies allowed industrial experiments, supported by National High-tech Research and Development Projects (863), to be conducted jointly by the ENN Group and China University of Mining and Technology between 2011 and 2014 (Kang and Liang 2011). In particular, four gasified working faces were studied at an experimental demonstration base in Ulan Qab, Inner Mongolia. Numerical methods were used to analyze the stress distribution in hyperbolic coking pillars to better understand the influence of both pillar dimensions and mechanical properties on their bearing capacity. Based on our findings, we propose a stability evaluation method and apply this model to a case study engineering project. Our results have important theoretical and practical implications for the promotion of UCG technology worldwide.

Materials and methods

Gasification technology

A schematic diagram of SMFM technology is shown in Fig. 1. The first implementation step includes drilling and combustion to form both gas removal and ignition channels. The starting point of the gasification process, labeled as a red circle (A) in Fig. 1, is then ignited, and the first working face is gasified in a retraction-controlled manner. The same approach is subsequently applied to additional working faces (e.g., second, third, and fourth gasification faces in Fig. 1). To verify the effectiveness and reliability of the SMFM, drill samples of the gasified coal pillar were collected and analyzed using energy disperse spectroscopy (EDS) (Fig. 2) (Bruker Quantax 400) (Meyer et al. 2012; Marras et al. 2013). The measured carbon content of lignite samples is found to decrease substantially after gasification, leaving mostly Si and Mg (Fig. 2), which verifies that SMFM can be used to extract energy from coal resources. The coal pillar formed by SMFM technology is hyperbolic, as shown in Fig. 3.

Numerical simulations

We performed numerical simulations to calculate bearing stresses resulting from different dimension-based variables (pillar height, width, and arch height) and mechanical properties (cohesion) using ANSYS and FLAC®3D software. The elastic-plastic limit equilibrium method (Fan 2004) was used to obtain the total bearing energy of the
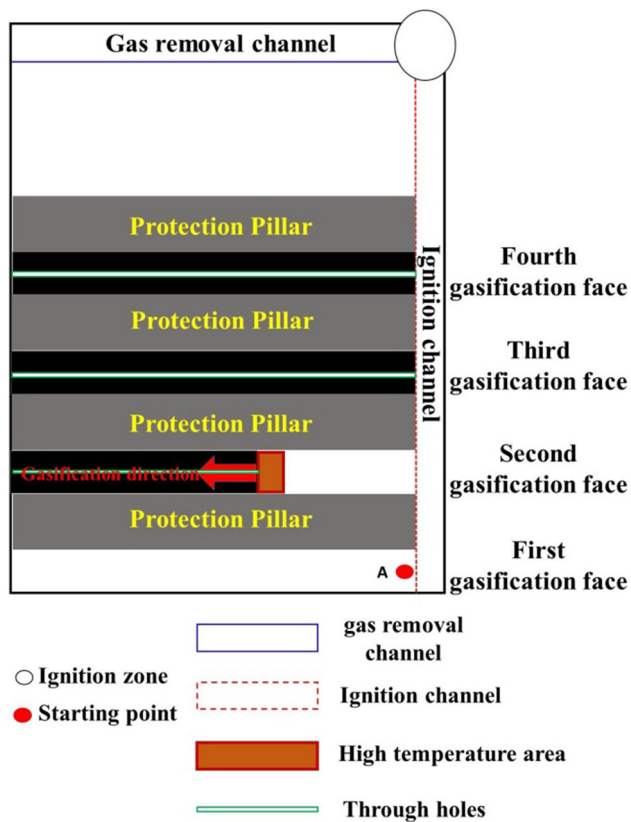
Fig. 1 Schematic diagram of the strip mining-face mining gasifier CRI underground gasification technology (SMFM)

pillars. Origin software was used to fit the results (Zhang et al. 2005; Yu et al. 2010).

In the dimension-based simulations, two variables were kept fixed (e.g., pillar height, width, or arch height) while a third varied over a range of values. The first set of simulations ($n = 6$) included variable arch height (0–2.5 m, 0.5-m increments) with a fixed pillar height and width of 5 and 10 m, respectively (Fig. 4). The second set ($n = 5$) included variable pillar width (10–50 m, 10-m increments) with fixed pillar and arch heights of 5 and 1.5 m, respectively (Figure 5). The third set ($n = 6$) included variable pillar height (4–10 m, 1-m increments) with fixed pillar width and arch height of 10 and 1.5 m, respectively (Fig. 6). In the material-based simulations ($n = 5$), dimensions were kept fixed (height: 5 m; width: 10 m; arch height: 1.5 m) while cohesion values varied from 0.6 times to 1.4 times in 0.2-MPa increments.

In all simulations, the pillar length was 100 m and the model bottom kept fixed. Geomechanical parameters were taken from experimental results of Tang (2013) obtained on coal samples from Ulan Qab (Table 1). These authors report that the large mechanical property changes of the pillars generally occur within the first 2–3 m on both sides of the combustion area. The depth of the cohesion property in the simulations was therefore set to within two meters.

Results

Our results indicate that pillar arch height has the strongest influence on its bearing capacity compared with other dimension-based variables (i.e., pillar height, width). It can be seen in Fig. 7 that stress decreases linearly (R^2 is 0.981) with increasing arch height, from $\sim$ 3.5 MPa in the arch-absent scenario (arch height = 0 m) to $\sim$ 1 MPa (arch height = 2 m). The relationship between stress and pillar width (Fig. 8) shows a much weaker effect, with stress increasing only slightly from $\sim$ 1 MPa (10-m width)

**Fig. 2** Energy spectrum analysis of coal samples after gasification
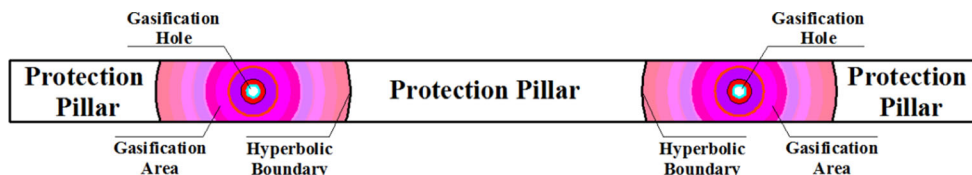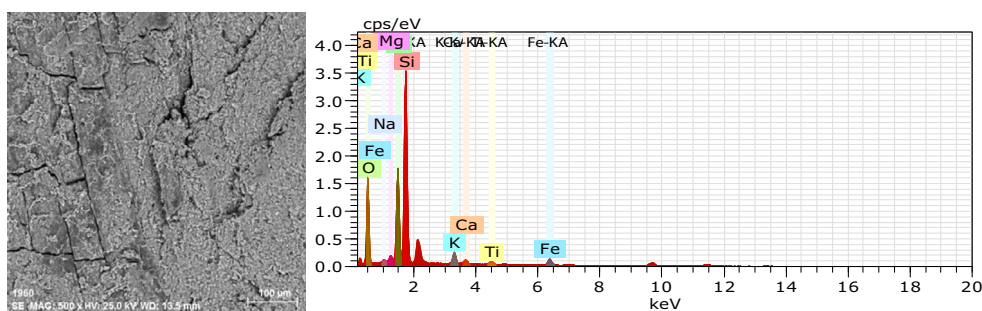
**Fig. 3** Physical structure of separated coal pillars after gasification

Fig. 4 Hyperbolic coal pillars with different arch heights. Pillar height and width are 5 and 10 m, respectively. **a** 2.5 m **b** 2 m **c** 1.5 m, **d** 1 m **e** 0.5 m **f** 0 m
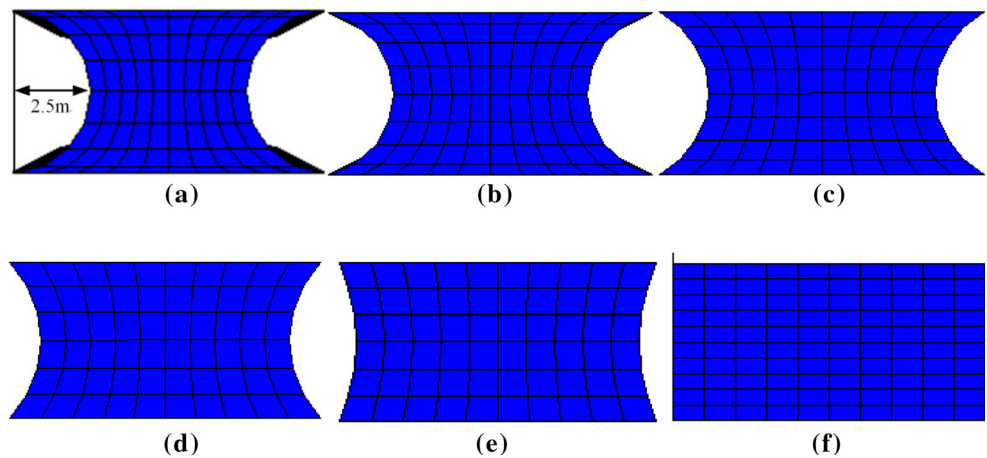
Fig. 5 Hyperbolic coal pillar models with different widths. Pillar height and arch height are 5 and 1.5 m, respectively. **a** 10 m **b** 20 m, **c** 30 m, **d** 40 m, **e** 50 m
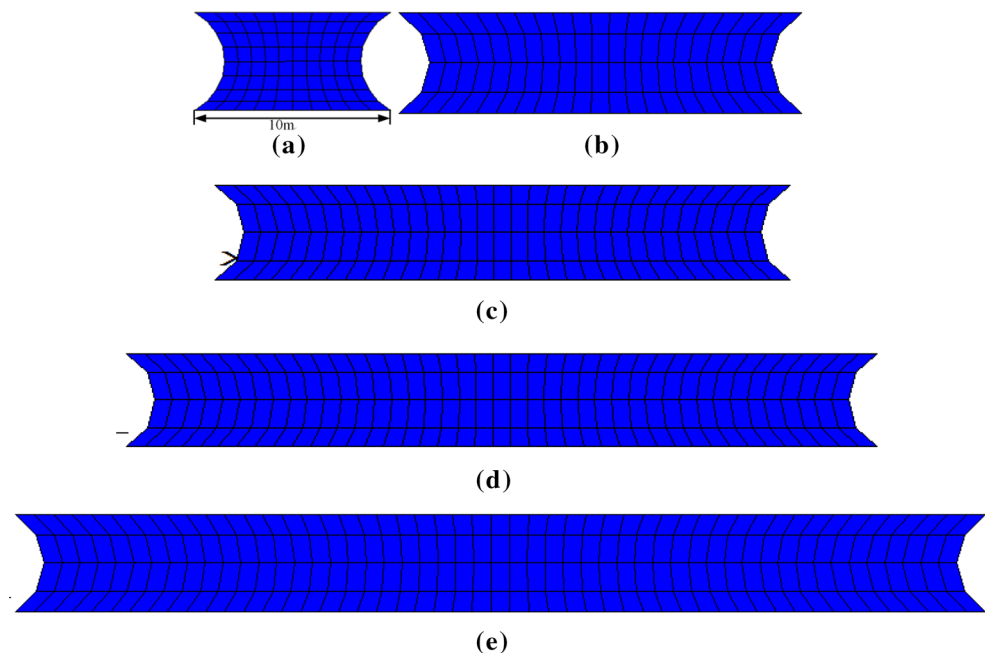
Fig. 6 Hyperbolic coal pillars with different heights. Pillar width and arch height are 5 and 1.5 m, respectively. **a** 4 m **b** 5 m **c** 6 m **d** 8 m **e** 10 m
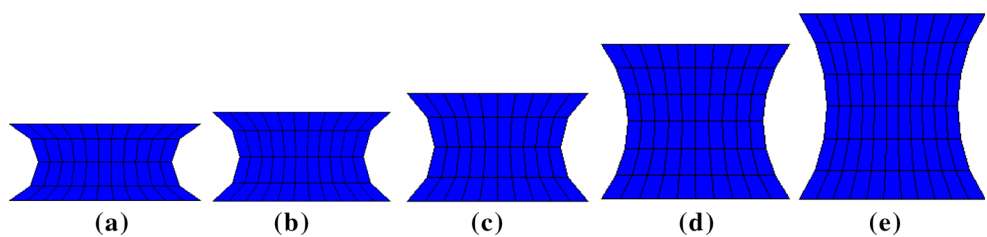

Table 1 Geomechanical parameters of the coal pillar used in this study

| Lithology	Elasticity modulus (GPa)	Poisson ratio	Tensile strength (MPa)	Cohesion (MPa)	Internal friction angle (°)
Coal	1.45	0.3	1	1	20

to $\sim$ 1.5 MPa (50-m width), and is better fitted with a logarithmic solution ($R^2 = 0.99$). Stress is also proportional to pillar height with a slightly stronger effect than pillar width, increasing from $\sim$ 1 MPa at 4-m height to $\sim$ 1.8 MPa at 10-m height. This relation is fitted by an exponential solution ($R^2 = 0.92$) (Fig. 9). The materials-
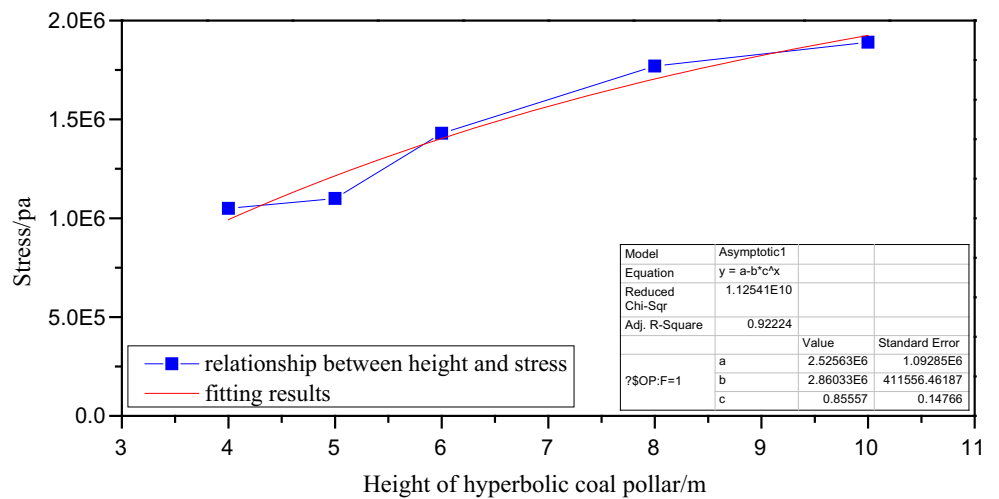
Fig. 7 Ultimate bearing capacity of hyperbolic pillars as a function of arch height. Pillar height and width are 5 and 10 m, respectively
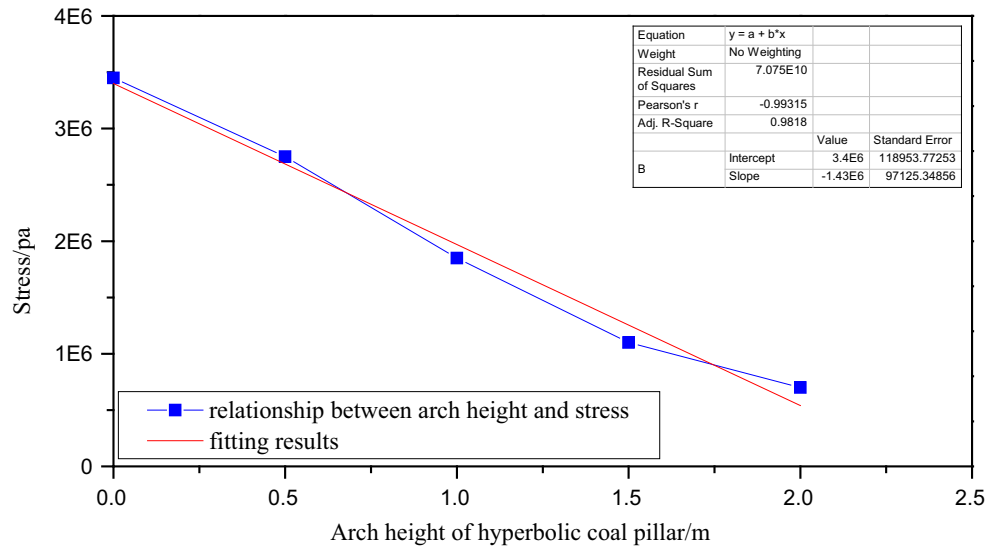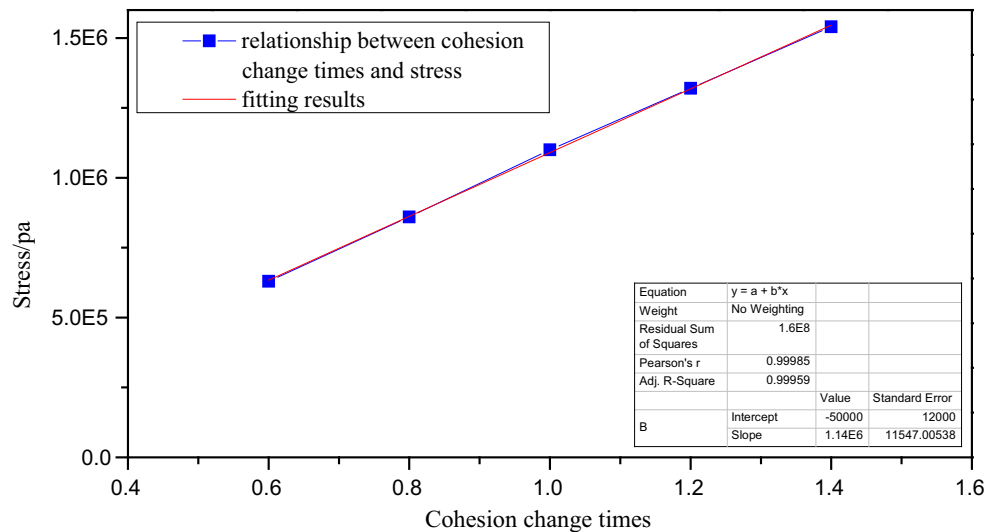

Fig. 8 Ultimate bearing capacity of hyperbolic pillars as a function of pillar width. Pillar height and arch height are 5 and 1.5 m, respectively
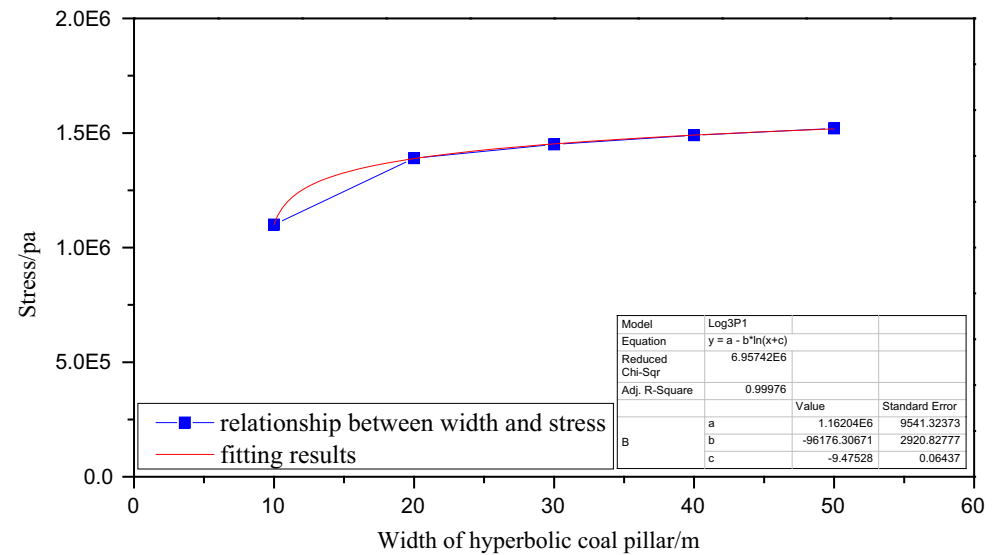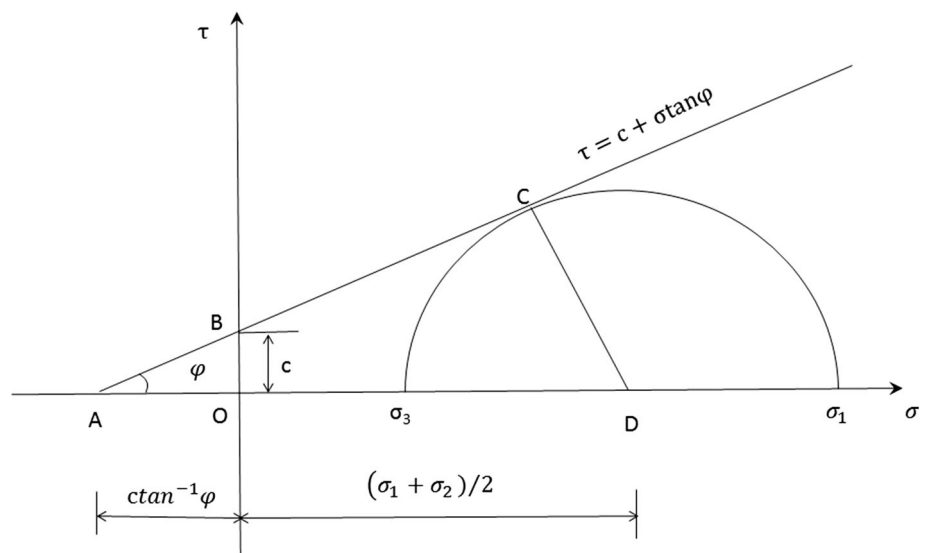

Fig. 9 Ultimate bearing capacity of hyperbolic pillars as a function of pillar height. Pillar width and arch height are 5 and 5 and 1.5 m, respectively

Fig. 10 Ultimate bearing capacity of hyperbolic pillars as a function of cohesion. The arch height is 1.5 m, and the pillar height and width are 5 and 10 m, respectively

Equation	y = a + b*x		
Weight	No Weighting		
Residual Sum of Squares	1.6E8		
Pearson's r	0.99985		
Adj. R-Square	0.99959		
		Value	Standard Error
B	Intercept	-50000	12000
	Slope	1.14E6	11547.00538

Fig. 11 Equilibrium conditions under a three-dimensional stress state

based results show that cohesion is also important, with the lowest of all measured stress values (~ 0.6 MPa) at low cohesion (0.6 times) increasing linearly ($R^2 = 0.99$) to ~ 1.5 MPa at higher cohesion (1.4 times) (Fig. 10).

Discussion

The design of stable and reasonably separated coal pillars for the implementation of SMFM is of critical importance. The results obtained in this study indicate that the bearing capacity of hyperbolic coal pillars is affected by its arch height, pillar height and width, and mechanical property changes. In this context, it is therefore necessary to further investigate a stability evaluation method of hyperbolic coal pillars to facilitate SMFM implementation in real projects.

We first review the mathematics of pillar bearing capacity in the conventional rectangular coal pillar ("Ultimate bearing capacity of a rectangle coal pillar" section), describe the bending and rectangular zones of hyperbolic pillars and proposed stability evaluation method ("Stability evaluation method of the hyperbolic coal pillar" section), and finally apply this model to a case study ("Case study" section).

Ultimate bearing capacity of a rectangle coal pillar

Equilibrium conditions under a three-dimensional stress state are shown in Fig. 11, according to Wang et al. (2002):

$$\frac{\sigma_1 - \sigma_2}{2} = \left[\frac{\sigma_1 - \sigma_2}{2} + c \tan^{-1} \varphi \right] \sin \varphi$$

$$\sigma_1 = \frac{2c\cos\varphi}{1 - \sin\varphi} + \frac{1 + \sin\varphi}{1 - \sin\varphi}\sigma_3 \qquad (1)$$

where c represents the pillar cohesion (MPa), φ is the pillar's internal friction angle (°), and σ_3 is the lateral stress (MPa), which is zero on the pillar edge. Lateral stress in the yielding zone increases from the outside inward and reaches its maximum at the junction of the nuclear zone, which then returns to the gravity stress of the pre-mining original rock ($\sigma_3 = \gamma H$), where γ is the average weight of the overlying strata (kg/m^3) and H is the mining depth.

Once the stress in the nuclear zone reaches its peak, the elastic state will gradually fade, causing instability in the pillar. The σ_3 value can then be substituted into Eq. (1) and the result is as follows:

$$\sigma_1 = \frac{2c\cos\varphi}{1 - \sin\varphi} + \frac{1 + \sin\varphi}{1 - \sin\varphi}\gamma H \qquad (2)$$

The φ value of the coal body is first set to 36°, following British standards, and the ultimate load-bearing strength is obtained by simplifying the first item on the right of Eq. (2) to ($\sigma_1 \approx 4\gamma H$). According to Wilson theory (Wilson 1983), the length L of a common strip coal pillar is far more than its width a and can be considered a problem of plane geometry. Neglecting the edge effect of the strip pillar, the ultimate bearing capacity can be described as follows:

$$\sigma_s = 4\gamma H(a - Y)L \qquad (3)$$

where Y represents the width of the plastic zone. The units of H, Y, and L are in meters. Using the relationship between Y and H, the coal seam thickness (m) was obtained by Wilson (1983) according to:

$$Y = 0.00492mH \qquad (4)$$

The result is obtained by substituting Eq. (4) into Eq. (3):

$$\sigma_s = 4\gamma H(a - 0.00492mH)L \qquad (5)$$

Wang et al. (2002) improved the Wilson (1983) formula and obtained a more reasonable ultimate bearing capacity for strip pillars according to:

$$\sigma_s = \left[\frac{2c\cos\varphi}{1 - \sin\varphi} + \frac{1 + \sin\varphi}{1 - \sin\varphi}\gamma H\right](a - 0.00492mH)L \qquad (6)$$

Stability evaluation method of the hyperbolic coal pillar

The hyperbolic coal pillar can be divided into a bending zone and rectangular zone, as shown in Fig. 12. The ultimate bearing load is therefore calculated in two parts. The pillar is stable when the real load of the bending zone is less than its ultimate bearing load, and when the real load

of the bending part is more than its ultimate bearing load, the pillar is unstable. To guarantee pillar stability, the real load of the rectangular zone should be less than its ultimate bearing load.

Stability of the pillar bending zone

As can be seen in Fig. 12, the structure of the pillar's bending zone is unstable. Some bending of the pillar will occur as shear failure under the influence of the overburden. One can assume that the ability of the pillar to support the overburden can be described in terms of bending part thickness (h). This assumption leads to the following relations:

$$\int_{h_1}^{\frac{m}{2}} \tau_{xz}\,dz = K_1\gamma H = \sigma_z \qquad (7)$$

$$h = \frac{m}{2} - h_1 \qquad (8)$$

$$\tau_{xz} = \sigma_x \tan\varphi + c \qquad (9)$$

$$\sigma_x = \lambda\sigma_z \qquad (10)$$

$$K_1 = \frac{2\sqrt{b^2 - \frac{m^2}{4}} + a}{2b - 2\sqrt{b^2 - \left(\frac{m}{2} - h\right)^2} + a} \qquad (11)$$

where b represents the combustion zone width (m), a is the protection pillar width (m), K_1 is the stress concentration coefficient, λ is the lateral pressure coefficient of coal seam where $\lambda = \mu/(1 - \mu)$ and μ is the average Poisson's ratio, and c and φ are the average cohesion and internal friction angle (°) of the pillar bending zone after gasification, respectively.

The following relationship is obtained based on Eqs. (7)–(11).

$$\lambda h \tan\varphi + \frac{hc\left[2b - 2\sqrt{b^2 - \left(\frac{m}{2} - h\right)^2} + a\right]}{\gamma H\left(2\sqrt{b^2 - \frac{m^2}{4}} + a\right)} = 1 \qquad (12)$$

The value of h is obtained by the iteration method. The pillar bending zone is stable when $h < m/2$ and unstable when $h > m/2$. An example of an unstable bending zone is shown in Fig. 13.

Stability of the rectangular zone

The rectangular part of hyperbolic pillar supports the overburden and the real load σ_{p2} according to:

$$\sigma_{p2} = \gamma\left[(a + b) \times H - \frac{b^2 \times \cot\delta}{4}\right]L \qquad (13)$$

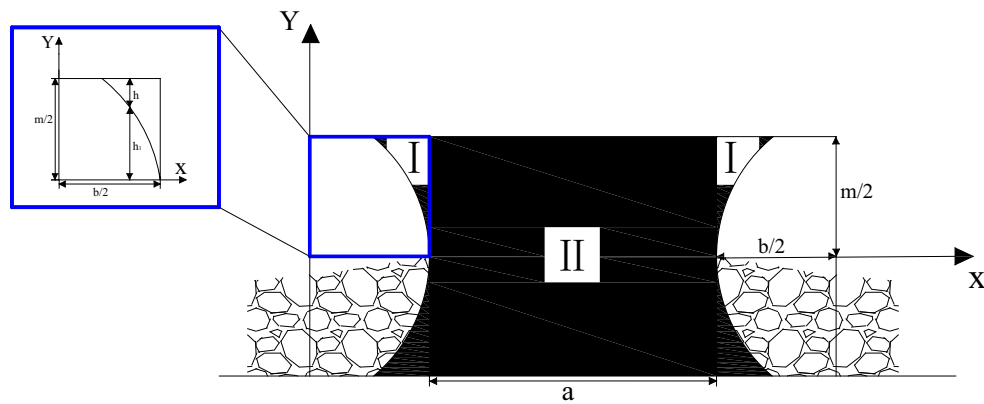where δ and γ are the caving angle (°) and average weight

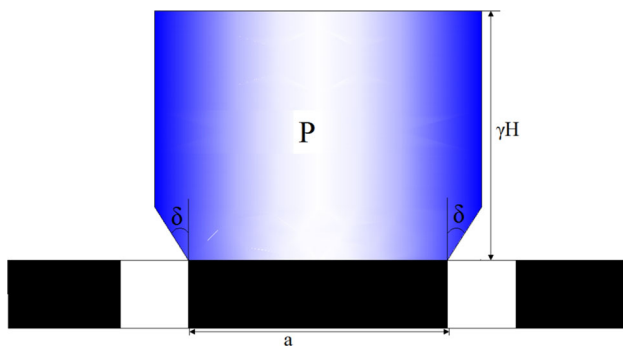**Fig. 12** Schematic diagram of a hyperbolic coal pillar

Fig. 13 Unstable bending zone of a hyperbolic coal pillar

(kg/m^3) of the combustion cavity overburden, respectively. The ultimate bearing load of the rectangular zone of the pillar is as follows:

$$\sigma'_s = \left[\frac{2c_1 \cos \varphi_1}{1 - \sin \varphi_1} + \frac{1 + \sin \varphi_1}{1 - \sin \varphi_1} \gamma H\right](a - 0.00492mH)L \tag{14}$$

where c_1 and φ_1 are the average cohesion and internal friction angle (°), respectively. To ensure the stability of the hyperbolic coal pillar, the following requirement must be met:

$$\frac{\sigma'_s}{\sigma_{p2}} = K > 1 \tag{15}$$

where K is the safety factor. Using the approach described here, stability can be evaluated and a retaining width with an appropriate K value chosen based on project needs. It is important to note that the stability evaluation method outlined here is intended for final pillar stability rather than stability during gasification. Following implementation of the SMFM, the temperature gradually reduces and eventually approaches the temperature of surrounding material, however, the mechanical properties of coal pillar and the surrounding rock change due to high temperature.

Therefore, the stability evaluation method presented here takes the mechanical properties of the pillars and overlying strata caused by high temperature into consideration and does not consider the temperature equation during the gasification process.

Case study

The SMFM configuration is currently only applied in a mine in China, so we select this location as our case study. The gasifier position and distribution are shown in Fig. 14. There are four working faces separated by a 24-m retaining width with a 16-m wide gasification channel and advancing length of 173 m. The average mining thickness is 5.5 m. The working faces are along flat lignite seams with an average mining depth of 275.75 m. On the basis of mechanical properties measured from experiments on coal seams in the area (Tang 2013), we use a cohesion value of
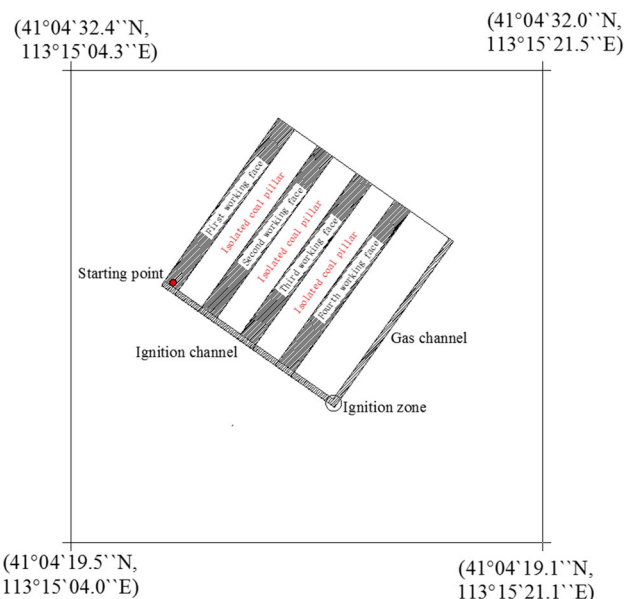

Fig. 14 Gasifier position and distribution

0.08 MPa and an internal friction angle of 33.28° before gasification. The specific gasification process is listed below.

1. The gas outlet channel was first processed after ignition. After 60 days, the gas channel had formed to a width of 5 m and length of 170 m.
2. The ignition channel was processed and after 60 days had formed with the same dimensions as in step 1.
3. Underground gasification on the first working face was carried out starting from the ignition channel until the end of the working face. After 90 days, a combustion cavity with a width of 16 m and length of 170 m had developed.
4. Gasification was carried out sequentially on the second, third, and fourth working faces. After 90 days, all cavities had developed to the same dimensions as in step 3.
5. The gasification process finished and gasifiers were closed.

No obvious surface subsidence was observed after gasification, which suggests that the retained coal pillars should be stable. The method proposed in this paper can be used to verify this assumption. As discussed in "Stability evaluation method of the hyperbolic coal pillar" section, the bending zone of the pillar can be neglected if the rectangular zone is able to support the overburden, at which point, the remaining pillars will be stable. The result is obtained by substituting the above data into Eq. (15), such that

$$K = \frac{\sigma'_s}{\sigma_{p2}} = 1.77 > 1$$

Our results verify that the coal pillars are stable in this industrial case study.

In this preliminary experiment of SMFM, we observed that the separation between the gasification working faces is relatively large, which ensures the stability of the separated pillars and gasifier, and causes no obvious surface subsidence. However, in the future promotion and application of this technology, the separated distance will need to be reduced to increases resource utilization. In general, the overall bearing capacity of the hyperbolic pillar needs to be considered to ensure stability and control surface subsidence, as well as to reduce the retaining width and improve resource utilization. The proposed stability evaluation method presented in this study aims to solve this problem.

Conclusions

We have performed numerical simulations to analyze the influence of different factors (arch height, pillar height and width, cohesion) on the ultimate bearing capacity of hyperbolic pillars in SMFM operations. The theoretical results are used to better understand the stress distribution of pillars under the coupling effect of high temperature and ground stress. The main conclusions of this study are listed below.

1. SMFM technology is an effective method for extracting valuable components from coal and leaving solid waste in the cavity. However, there are important differences between the hyperbolic coking pillars (or semi-coking) used in SMFM operations compared with rectangular pillars used in conventional strip mining.
2. The arch height, pillar height and width, and mechanical properties of a hyperbolic pillar have an influence on its ultimate bearing capacity. The bearing capacity has a linear inversely relationship with its arch height, a logarithmic relationship with pillar width, an exponential relationship with pillar height, and a positive linear relationship with its cohesion.
3. The proposed stability evaluation method can be used to predict the stability of hyperbolic coal pillars. This method can therefore be used to design the proper retaining width with an appropriate safety factor (K). The coal pillars in our industrial case study remained stable; a result that is verified using the proposed stability evaluation method.

References

Bhutto AW, Bazmi AA, Zahedi G (2013) Underground coal gasification: from fundamentals to applications. Prog Energy Combust Sci 39(1):189–214

Couch GR (2009) Underground coal gasification. IEA Clean Coal Center, International Energy Agency, London. ISBN 978-92-9029-471-9

Derbin Y, Walker J, Wanatowski D, Marshall A (2015) Soviet experience of underground coal gasification focusing on surface subsidence. J Zhejiang Univ Sci A 16(10):839–850

Fan JT (2004) Slope stability analysis of complex rock by elastic-plastic limit equilibrium method. Central South University **(in Chinese)**

Gao W (2014) Study on the width of the non-elastic zone in inclined coal pillar for strip mining. Int J Rock Mech Min Sci 72:304–310

Guo W, Wang H, Chen S (2016) Coal pillar safety and surface deformation characteristics of wide strip pillar mining in deep mine. Arab J Geosci 9(2):1–9

Kang SY, Liang ZR (2011) Underground coal gasification: safety, efficiency and green coal mining technology-an interview of

Liang Jie, the director of coal underground gasification engineering research center of china university of mining and technology (Beijing) and chief scientist of ENN smart energy group. China Coal 37(1):12–14 **(in Chinese)**

Khadse A, Qayyumi M, Mahajani S et al (2007) Underground coal gasification: a new clean coal utilization technique for India. Energy 32(11):2061–2071

Klimenko Alexander Y (2009) Early ideas in underground coal gasification and their evolution. Energies 2(2):456–476

Li H, Guo G, Zhai S (2016) Mining scheme design for super-high water backfill strip mining under buildings: a Chinese case study. Environ Earth Sci 75(12):1–12

Marras C, Rizzi M, Ravagnan L, De Benedictis A, Zorzi G, Bongiorno G, Marchesi D, Messina G, Cordella R, Franzini A (2013) Morphological and chemical analysis of a deep brain stimulation electrode explanted from a dystonic patient. J Neural Transm 120(10):1425–1431

McInnis J, Singh S, Huq I (2016) Mitigation and adaptation strategies for global change via the implementation of underground coal gasification. Mitig Adapt Strat Glob Change 21(4):479–486

Meyer M, Schiffbauer JD, Xiao S, Cai Y, Hua H (2012) Taphonomy of the upper Ediacaran enigmatic ribbonlike fossil Shaanxilithes. Palaios 27(5):354–372

Prabu V, Jayanti S (2011) Simulation of cavity formation in underground coal gasification using bore hole combustion experiments. Energy 36(10):5854–5864

Prabu V, Jayanti S (2012) Laboratory scale studies on simulated underground coal gasification of high ash coals for carbon-neutral power generation. Energy 46(1):351–358

Shafirovich E, Varma A (2009) Underground coal gasification: a brief review of current status. Ind Eng Chem Res 48(17):7865–7875

Siemens CW (1868) XXXIII—on the regenerative gas furnace as applied to the manufacture of cast steel. J Chem Soc 21:279–310

Stańczyk K, Howaniec N, Smoliński A, Świądrowski J, Kapusta K, Wiatowski M, Grabowski J, Rogut J (2011) Gasification of lignite and hard coal with air and oxygen enriched air in a pilot scale ex situ reactor for underground gasification. Fuel 90(5):1953–1962

Stuermer DH, Ng DJ, Morris CJ (1982) Organic contaminants in groundwater near an underground coal gasification site in northeastern Wyoming. Environ Sci Technol 16(9):582–587

Tang FR (2013) Fracture evolution and breakage of overlying strata of combustion space area in underground coal gasification. China University of Mining and Technology **(in Chinese)**

Walker LK, Blinderman MS, Brun K (2001, October) An IGCC project at Chinchilla, Australia based on underground coal gasification (UCG). In: 2001 Gasification technologies conference, San Francisco

Wang XC, Huang FC, Zhang HX, Zhang LG (2002) Discussion and improvement for A.H.Wilsons coal pillar design. J China Coal Soc 27(6):604–608 **(in Chinese)**

Wang ZT, Fu ZK, Jiao JL, Li DH, Huo LW (2008) Micro-seismic monitoring on position situation of flame working face in underground coal gasification. J Min Saf Eng 25(4):394–399 **(in Chinese)**

Wilson AH (1983) The stability of underground workings in the soft rocks of the coal measures. Int J Min Eng 1(2):91–187

Xin L (2014) Study on the overlying strata movement by UCG mining in Matigou Coal Mine. China University of Mining and Technology

Xin L, Wang ZT, Huang WG, Li XQ, Zhang P, Wang JH (2013) Study on underground coal gasification production and power generation experiment in Huating Area. Coal Sci Technol 41(05):28–34 **(in Chinese)**

Yang LH, Liang J, Yu L, He GX (1998) Industrial experiment of underground coal gasification. J China Univ Min Technol 27(3):254–256 **(in Chinese)**

Yang LH, Liang J, Yu L, Qin ZH (2000) The test study on underground coal gasification at Mazhuang Coal Mine in Xuzhou. J China Coal Soc 25(1):86–90 **(in Chinese)**

Yang L, Zhang X, Liu S, Yu L, Zhang W (2008) Field test of large-scale hydrogen manufacturing from underground coal gasification (UCG). Int J Hydrogen Energy 33(4):1275–1285

Yu W, Yun H, Zhongyi C, Zurong Y (2010) Application of origin software to experimental data fitting in chemical engineering principle. Exp Technol Manag 1:028

Zamzow KL (2010) Underground coal gasification. In: History, environmental issues, and the proposed project at Beluga, Alaska. Center for Science in Public Participation

Zhang Y, Cheng G, Ma W (2005) Analysis of fitting isotherm model using origin software. Comput Appl Chem 22(10):899